Received: Added at production | Revised: Added at production | Accepted: Added at production

FERMILAB-PUB-20-319-AE-SCD
ACCEPTED

DOI: xxx/xxxx

ARTICLE TYPE

Detailed Modeling of the Video Signal and Optimal Readout of Charge Coupled Devices

Fernando Chierchie*[1] | Guillermo Fernandez Moroni[1,3] | Pedro Querejeta Simbeni[1] | Leandro Stefanazzi[1,3] | Eduardo Paolini[1,4] | Miguel Sofo Haro[2,3] | Gustavo Cancelo[3] | Juan Estrada[3]

[1]Instituto de Investigaciones en Ingeniería Eléctrica “Alfredo Desages” and Depto. de Ing. Eléctrica y de Computadoras, CONICET and Universidad Nacional del Sur, Bahía Blanca, Prov. Bs.As., Argentina
[2]Centro Atómico Bariloche, Instituto Balseiro, Comisión Nacional de Energía Atómica (CNEA) and CONICET, Río Negro, Argentina
[3]Fermi National Accelerator Laboratory, Department of Energy, Illinois, United States
[4]Comisión de Investigaciones Científicas de la Provincia de Buenos Aires (CIC), Prov. Bs.As., Argentina

Correspondence
*Fernando Chierchie, Instituto de Investigaciones en Ing. Eléctrica (IIIE) “Alfredo Desages” (UNS-CONICET), Depto. de Ing. Eléctrica y de Computadoras, Universidad Nacional del Sur, Av. Alem 1253, Postal code: 8000, Bahía Blanca, Argentina. Email: fernando.chierchie@uns.edu.ar

Summary

This article provides a practical design methodology to calculate an optimal filter for noise reduction in the readout of charge-coupled devices (CCDs) taking into account the charge transfer and feedthroughs due to capacitive coupling in the CCD. A detailed analysis of the dynamics of the video signal and charge transfer is presented, including the circuital modeling of the output stage of the CCD and the dynamics of the electronics in the video chain before the analog to digital (AD) converter. This model is used to compute an optimal filter that minimizes the variance of the pixel noise and uses the samples of the charge transfer, before the charge is fully settled. This is necessary to enhances the performance of previous results that also use optimal filters but do not use the transition samples, while also reducing the pixel readout time, resulting in faster readouts. As a proof of concept for the optimal filter, we present novel experimental results using a Skipper CCD, which has a floating sense node that allows to measure the charge packet an arbitrary number of times. However, this technique can be applied to any CCD which has a readout system that digitally samples the video signal.

KEYWORDS:
CCD, readout, optimal filter, minimum noise variance, charge transfer

1 | INTRODUCTION

Image sensors are continuously evolving to produce faster and more accurate camera systems. The main objectives are to obtain low noise, high linearity and good dynamic range [1]. There are different technologies for image sensors, the two most popular being complementary metal-oxide semiconductor CMOS image sensors (CIS) and charge coupled devices (CCDs). CIS find applications in different fields such as surveillance, intelligent vision, massive consumer electronics, etc. [1] while CCDs are used mostly for scientific instruments. Different approaches have been reported in the literature to improve the performance of image sensors. Detailed modelling of the physical aspects and more complex sampling schemes were presented [2]. For sensitive applications that require high resolution, special circuits to convert the charge packet in each pixel into a digital word with constant resolution in a wide range of charges were studied [3]. The source follower buffer present in many image sensors to read the charge is one of the main sources of noise and nonlinearity. Some approaches study circuital modification to this output transistor [4] to enhance its performance. Other researchers seek to minimize the data rate and maximize the acquisition speed by

This manuscript has been authored by Fermi Research Alliance, LLC under Contract No. DE-AC02-07CH11359 with the U.S. Department of Energy, Office of Science, Office of High Energy Physics.

developing event-based image sensors [5] which use the same type of intelligence to acquire images only when something relevant is detected.

Charge Coupled Devices (CCDs) have dominated the sensor field in astronomical applications for many decades. The good gain uniformity and low noise obtained in the pixel readout of the array still makes them the first option for new instruments being built in the near future [6,7]. Moreover, the capability of the Skipper CCD [8,9] of multiple, independent readouts of the same pixel charge packet using a non-destructive process, allows for single photon discrimination. This opens new science possibilities for astronomical instruments. The drawback of the sensor is its long readout time given by the sequential pixel readout through a single amplifier (or just a few of them). The inverse relationship between the pixel error (readout noise) and the readout time per pixel results in a trade off that should be optimized to get the best outcome for each application. Any new technique that reduces the noise without increasing the readout time (or vice versa) can have a huge impact on current and new CCD based systems [10]. Recently, results that seek to optimize the readout time for a 3.2 gigapixel CCD array requiring a detailed modeling of the CCD video signal have been presented [11].

With the advancement of digital readout systems for CCDs many efforts have been reported in the literature to design digital filters to reduce the readout noise. Those filters use optimally computed coefficients to weight the samples of the video signal, unlike the standard digital version of correlated double sampling (CDS), which averages the signal and pedestal (reference level) levels and subtracts them to compute the pixel value. The digital CDS can be viewed as a FIR filter with coefficients taking constant values, while the optimal filter has coefficients whose value depend on the characteristic of the system noise.

Most of the attempts reported in the literature for optimal filtering [12,10,13,14,15] compute the coefficients without considering the samples between the signal and pedestal level, adding a gap (zero valued coefficients) between the coefficients of the optimal filter to avoid the transient samples. This gap dramatically deteriorates the practical performance of the filter as described in [14].

A more recent approach [16] develops the theoretical framework to compute an optimal filter considering the samples between the pedestal and signal level. This approach is validated via simulation results and considers a simple circuital model without clock feedthroughs. In this paper we extend the results in [16] by developing a practical approach for computing the coefficients using closed form expressions based on the measured noise. To achieve these results, we expand the developments of [17] with a more detailed modeling of the electrical characteristic of the output stage of the CCD that includes the feedthrough appearing in the video signal, and introducing a methodology to measure the noise.

The organization of this article is as follows: first the charge transport in the output stage of the CCD, the readout procedure and its electronic noise are modeled in Section 2. In the same section, the digital computation of the pixel value, incorporating the model of the CCD is discussed. The technique to obtain the coefficients of the optimal filter is developed in Section 3 where the standard CDS technique is reviewed in the context of digital filtering and charge transfer modeling. Section 4 presents simulations results and qualitative comparisons to previous results in the literature. Finally in Section 5, an experimental proof of concept to verify the model and the performance of the proposed optimal technique, and its comparison with standard CDS readout technique is developed using measured video and noise signals from an actual experimental setup. A practical method to measured representative system noise to compute the optimal filter coefficients is also presented.

2 | THEORETICAL MODEL FOR THE CHARGE-TRANSFER

In order to compute an optimal filter that takes into account the charge-transfer characteristics, it is necessary to model the CCD-output stage. The system diagram is depicted in Fig. 1, which shows the horizontal clocks gates $H1$, $H2$ and $H3$, the Summing Well (SW) with its clock signal V_{SW} and the Output Gate (OG) with its clock signal V_{OG}. It also shows the sense node (SN) to which the output amplifier is connected. This amplifier is polarized by the power supply V_{DD} and the external resistor R_L. The reset transistor, which operates as a switch, is connected to the power supply V_R and it is driven by the clock signal V_{RG}. In our experimental setup, both transistors are depletion p-type MOSFETs (a detailed analysis can be found in [18]) and charge carrier are holes (positive charge), but the analysis in this paper is general enough to be applied to any CCD even if the charge carriers are electrons. Fig. 1 also illustrates the movement of charge from the SW to the SN through the OG. When the potential of the SW is below the OG potential, the charge stays in the SW and when the potential of the SW is higher, charge will move from the SW to the SN.

The behavior of the output stage in Fig. 1 can be modeled by the circuit shown in Fig. 2 which, for simplicity, does not include the internal resistances of the sources and of the reset transistor, although they are part of the real circuit. All the dynamics is concentrated in the transfer function $G(s)$.

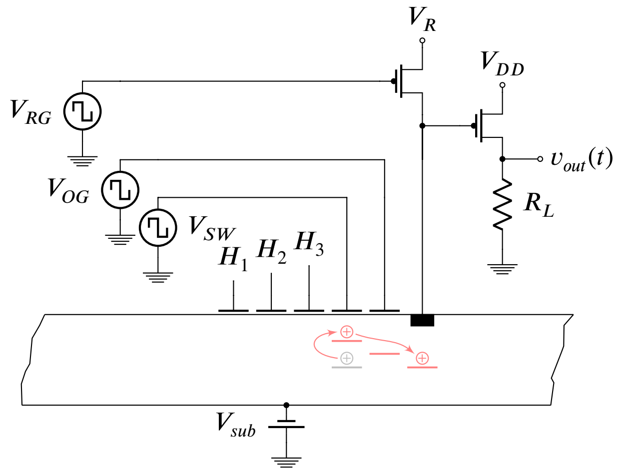

FIGURE 1 CCD output stage including the output transistor amplifier and reset transistor. Also shown are the horizontal clocks (H_1, H_2 and H_3), the summing well (SW), output gate (OG) and reset gate (RG). The sense node (SN) is indicated with a dark rectangle. The movement of charge (holes in our CCD) from the SW to the SN through the OG is also illustrated.

In the final stage of the readout process, the charge reaches the SW. At this point the SN is reset applying a pulse V_{RG} to the gate of the reset transistor, producing a pulse $v_{out,RG}(t)$ in the video signal $v_{out}(t)$ at the output of the source follower, as shown in Fig. 3(a). After the reset, the SN is charged to a constant level P with an uncertainty known as "reset noise". The time interval after the reset pulse and before the SW pulse is known as the "pedestal level", in which the reference voltage of the SN is measured, usually by integration during certain amount of time, if the readout is performed in the analog domain. After the pedestal, a pulse V_{SW} is used to transfer the charge from the SW to the SN. Even if no charge is present in the SW (empty pixel), the pulse V_{SW} produces a pulse in the video signal $v_{out}(t)$, shown in Fig. 3(a) and labeled $v_{out,SW}(t)$, caused by the capacitive coupling between the SW and the SN, modeled as $C1$ in Fig. 2. When there is charge in the pixel, it is transferred from the SW to the SN an instant after the SW pulse at t_0. This is modeled by the current source $i_Q(t)$ in Fig. 2 shown as an impulse in Fig. 3(a). This current source produces an a step voltage $v_{out,iQ}(t)$ with height equal to the pixel value (ΔV) in $v_{out}(t)$, which is known as the "signal level". In analog readout systems, the signal level is integrated after the charge is established, and subtracted to the integrated pedestal level to compute the pixel value ΔV, a process known as dual slope integration.

All three waveforms superimposed produce the video signal

$$v_{out}(t) = v_{out,RG}(t) + v_{out,SW}(t) + v_{out,iQ}(t) \tag{1}$$

at the output of the CCD.

It worth noting that signal $v_{out,RG}(t)$ is not the clock signal V_{RG}, which is applied to the gate of the reset transistor, but represents its contribution to the output signal $v_{out}(t)$. When V_{RG} is applied to the reset transistor, it generates a pulse at the sense node (SN) and this pulse is reflected in the output by the source follower transistor. In the same vein, signal $v_{out,SW}(t)$ is not the clock signal V_{SW} directly but represent the contribution of V_{SW} that passes through the capacitive impedance divider formed by capacitors $C1$ and SN capacitor and is reflected in the output by the source follower transistor. In other words, due to the intrinsic capacitive coupling that exists in charge coupled devices, the coupling between the RG and SW clocks and the output is considered as part of the ideal model.

Fig. 2 also includes the transfer function $G(s)$ which models the additional gain and filtering (bandwidth limit) of the electronic chain before the analog dual slope integrator or ADC converter (in the case of digital readout). Signals $v_{out,RG}(t)$, $v_{out,SW}(t)$ and $v_{out,iQ}(t)$ after the transfer function $G(s)$ are labeled as $v_{o,RG}(t)$, $v_{o,SW}(t)$ and $v_{o,iQ}(t)$ respectively, which are shown in Fig. 3(b). The resultant video signal, produced by the superposition of the three waveforms, is shown in Fig. 3(c).

Modeling the noise of the system as $v_\eta(t)$ and adding it to the output voltage results in

$$v_o(t) = v_{o,SW}(t) + v_{o,RG}(t) + v_{o,iQ}(t) + v_\eta(t), \tag{2}$$

where $v_{o,SW}(t)$ can be considered a deterministic function, $v_{o,RG}(t)$ is a negative pulse that achieves a stationary value, the "pedestal level" when the transient ends, which has an uncertainty known as the "reset noise"[19]. This means that the pedestal

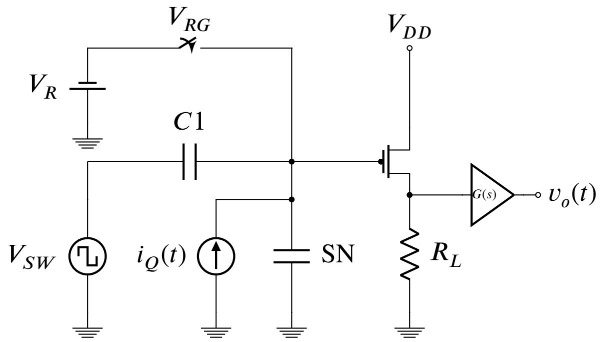

FIGURE 2 Circuit model taking into account capacitive coupling C_1 between Summing Well (SW) and Sense Node (SN).The impulsive source $i_Q(t) = I_o\delta(t-t_0)$ represents the charge transfer from SW to SN at time t_0. In this circuit, the internal resistances of the sources and of the reset transistor have been omitted for simplicity, although they are part of the real circuit.

level is constant within a pixel interval but may change from pixel to pixel. Fig. 3(d) illustrates qualitatively the effect of the noise signal $v_\eta(t)$ into the video signal.

Only the term $v_{o,iQ}(t)$ depends on the pixel charge and can be approximated as

$$v_{o,iQ}(t) = \begin{cases} 0 & \text{if } t < t_0 \\ \Delta V\left(1 - e^{-\frac{t-t_0}{\tau}}\right) & \text{if } t \geq t_0 \end{cases} \tag{3}$$

where t_0 is the instant at which the charge transfer starts and τ the time constant of the assumed first order transfer function $G(s)$ for the video signal chain. The experimental sections show that the first order dynamic assumption, also used in[16] is accurate enough for our experimental setup. If significant higher order dynamics are involved then it should be modeled and added to (3).

2.1 | Digital computation of the pixel value

The signal $v_o(t)$ is sampled with a sampling frequency $F_s = 1/T_s$ using an analog to digital converter. The discrete time signal $v_o[n] = v_o(nT_s)$ is then

$$v_o[n] = v_{o,SW}[n] + v_{o,RG}[n] + v_{o,iQ}[n] + v_\eta[n]. \tag{4}$$

Without loss of generality we consider that the time t_0 when the charge is transferred form the SW to the SN is $t_0 = (N+1)T_s$. The discrete-time signal $v_o[n]$ is used to compute the pixel value. The samples of $v_o[n]$ that are used to compute the pixel $\hat{P}_i$ are $v_o^i[n]$ with $n = 1 \cdots 2N$. This samples are indicated in Fig. 3(c) with red circles for $n = 1 \cdots N$ and green circles for $n = (N+1) \cdots 2N$, excluding the samples at the beginning of the pixel in the reset pulse transient.

The pixel value is computed as

$$\hat{P}_i = \sum_{k=1}^{2N} h_k v_o^i[k] \tag{5}$$

where h_k are the filter coefficients (to be determined) that minimize the pixel error produced by the noise signal $v_\eta[n]$, which we assume has zero mean. Notice that in this development, all the samples of the video signal, including those of the transition from the pedestal to the signal level are used.

The expected pixel value can be computed as

$$\begin{aligned} E(\hat{P}_i) &= E\left(\sum_{k=1}^{2N} h_k v_o^i[k]\right) \\ &= E\left(\sum_{k=1}^{2N} h_k (v_{o,SW}^i[k] + v_{o,iQ}^i[k] + v_{o,RG}^i[k] + v_\eta^i[k])\right) \\ &= K_{SW} + \sum_{k=1}^{2N} h_k E\left(v_{o,iQ}^i[k]\right) + \sum_{k=1}^{2N} h_k E\left(v_{o,RG}^i[k]\right), \end{aligned} \tag{6}$$

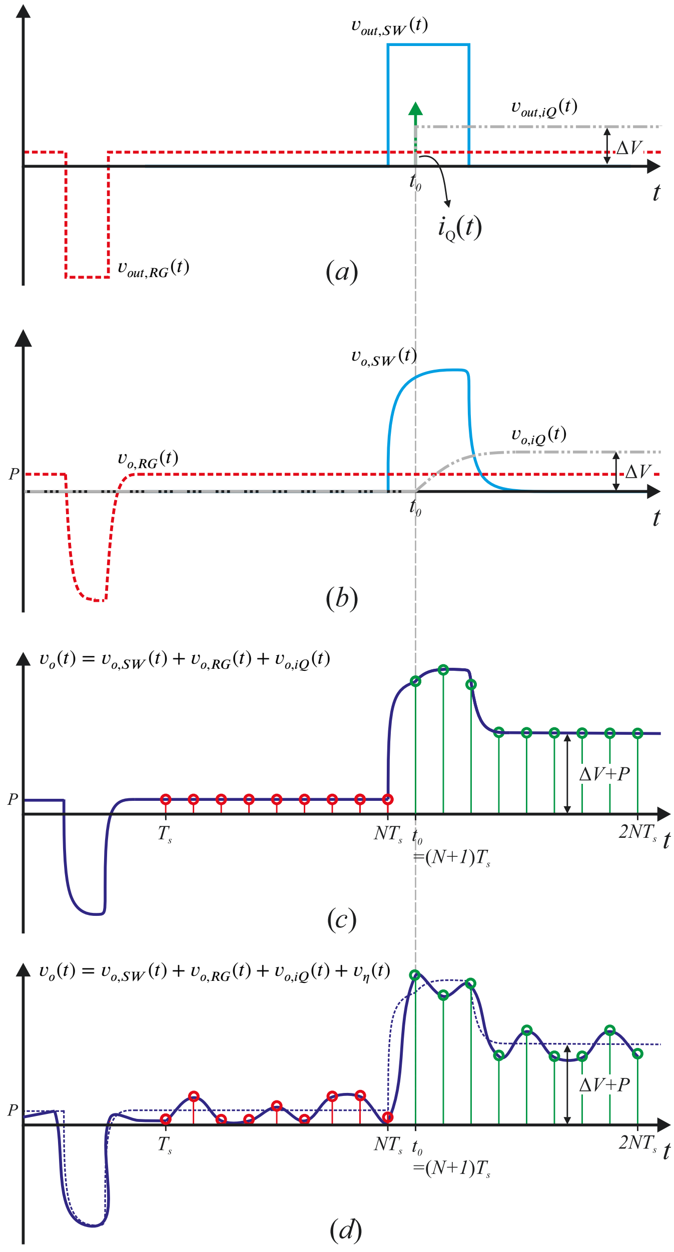

FIGURE 3 Illustration of video signal construction by superposition of three waveforms produced by the reset-gate feedthrough $v_{o,RG}(t)$, the summing well feedthrough $v_{o,SW}(t)$ and by the charge $v_{o,iQ}(t)$. (a) ideal waveforms without dynamics; (b) real waveforms; (c) resultant video signal without noise; (d) video signal with noise.

where $K_{SW} = \sum_{k=1}^{2N} h_k E\left(v^i_{o,SW}[k]\right)$ is a constant offset in the pixel value produced by the summing well feedthrough in the video signal. Note that $v^i_{o,iQ}[k] = 0$ for $0 \leq k \leq N$, and in the interval $N+1 \leq k \leq 2N$ is given by the samples of (3) at $t = kT_s$. Therefore,

$$\sum_{k=1}^{2N} h_k E(v^i_{o,iQ}[k]) = \sum_{k=N+1}^{2N} h_k \Delta V \left(1 - e^{-\frac{k-n_0}{n_1}}\right) \tag{7}$$

where $n_0 = N+1$ is the delay in samples ($t_0 = (N+1)T_s$), and $n_1 = \tau/T_s$ is the exponential time constant in samples. The third term in (6) is the (filtered) value of the pedestal level, which is considered a random variable that can varies from pixel to pixel but not inside the pixel. The expected value of this random variable is $E(v^i_{o,RG}[k]) = P$. Then,

$$\sum_{k=1}^{2N} h_k E(v^i_{o,RG}[k]) = \sum_{k=1}^{2N} h_k P. \tag{8}$$

From (6), (7) and (8), the expected pixel value can be written as

$$\begin{aligned} E(\hat{P}_i) &= K_{SW} + \Delta V \sum_{k=N+1}^{2N} h_k \left(1 - e^{-\frac{k-n_0}{n_1}}\right) + P \sum_{k=1}^{2N} h_k \\ &= K_{SW} + E(P_i) \end{aligned} \tag{9}$$

where $E(P_i) = E(\hat{P}_i) - K_{SW}$ is the expected value of the pixel without the constant K_{SW}.

3 | OPTIMAL FILTER COMPUTATION

The K_{SW} offset is the same for every pixel and therefore it does not introduce statistical uncertainty in the measurement of the charge packet. The value can be calculated using standard tools and subtracted from all the pixels of the images [19], so it will be discarded for the rest of the analysis and $E(P_i)$ will be used instead of $E(\hat{P}_i)$. Equation (9) can be reformulated using vectors and matrix notation as

$$E(P_i) = \Delta V \mathbf{h}^T \mathbf{e_2} + P \mathbf{h}^T \mathbf{e_1} \tag{10}$$

where

$$\mathbf{e}_1^T = [\underbrace{1, 1, \cdots, 1, 1}_{2N}], \tag{11}$$

$$\mathbf{e}_2^T = [\underbrace{0, 0 \cdots, 0}_{N}, \underbrace{0, 1 - e^{-\frac{1}{n_1}}, 1 - e^{-\frac{2}{n_1}} \cdots, 1 - e^{-\frac{N-1}{n_1}}}_{N}] \tag{12}$$

and $\mathbf{h} = [h_1, h_2, \cdots, h_{2N}]^T$ is the vector of coefficients of the filter.

3.1 | Pixel Variance

The effect of the electronic noise produced on the CCD readout can be characterized by quantifying the variance of the pixel error. The optimal filter is calculated by minimizing the pixel variance.

As explained before, the proposed filter does not discard the intermediate samples from the settling times of the charge signal. Setting the expected value in (10) equal to ΔV gives:

$$\Delta V = P \mathbf{h}^T \mathbf{e_1} + \Delta V \mathbf{h}^T \mathbf{e_2}. \tag{13}$$

In order to have $E(P_i) = \Delta V$, the filter has to fulfill the constrains

$$\begin{aligned} \mathbf{h}^T \mathbf{e_1} &= 0 \\ \mathbf{h}^T \mathbf{e_2} &= 1. \end{aligned} \tag{14}$$

Now, considering equation (5) in matrix form, the value of the i−th pixel P_i is (without considering the constant K_{SW})

$$P_i = \mathbf{v_o^i}^T \mathbf{h}, \tag{15}$$

where $\mathbf{v_o^i}^T = [v^i_o[1], v^i_o[2], \cdots, v^i_o[2N]]^T$ is the vector of samples of the video signal used to compute the pixel P_i. The variance is

$$\begin{aligned} \mathrm{Var}(P_i) &= E\left((P_i - E(P_i))^2\right) \\ &= E\left((\mathbf{v_o^i}^T \mathbf{h} - \Delta V)^2\right) \\ &= E\left(\left((\hat{\mathbf{v}}_\mathbf{o}^\mathbf{i} + \boldsymbol{\eta})^T \mathbf{h} - \Delta V\right)^2\right) \end{aligned} \tag{16}$$

where $\hat{\mathbf{v}}_{\mathbf{o}}^{\mathbf{i}}$ is the vector of video samples without noise and $\boldsymbol{\eta}^T = [v_\eta[1], \cdots, v_\eta[N], v_\eta[N+1], \cdots, v_\eta[2N]]$ is the vector of noise samples. If we consider $\mathbf{h}^T$ as an unbiased estimator: $(\hat{\mathbf{v}}_{\mathbf{o}}^{\mathbf{i}})^T\mathbf{h} = \Delta V$, is possible to compute $\mathrm{Var}(P_i)$ as

$$\mathrm{Var}(P_i) = E\left((\boldsymbol{\eta}^T\mathbf{h})^2\right) = \mathbf{h}^T E\left(\boldsymbol{\eta}\boldsymbol{\eta}^T\right)\mathbf{h} = \mathbf{h}^T\mathbf{R}\mathbf{h} \tag{17}$$

where R is the auto-correlation matrix of the noise vector $\boldsymbol{\eta}^T$.

3.2 | Minimization of the noise variance

The optimal filter coefficients can be computed by minimizing the objective function (J) subject to the restrictions in (14), following the procedure in [15]

$$J = \mathbf{h}^T\mathbf{R}\mathbf{h} - \lambda_1\mathbf{h}^T\mathbf{e}_1 - \lambda_2\left(\mathbf{h}^T\mathbf{e}_2 - 1\right). \tag{18}$$

where λ_1 and λ_2 are the Lagrange Multipliers. To find the optimal filter coefficients we equate to zero the derivatives of J with respect to $\mathbf{h}$, λ_1 and λ_2,

$$\frac{\partial J}{\partial \mathbf{h}} = 2\mathbf{h}^T\mathbf{R} - \lambda_1\mathbf{e}_1^T - \lambda_2\mathbf{e}_2^T = \mathbf{0}^T. \tag{19}$$

This minimization results in

$$\mathbf{h}^T = \frac{1}{2}\left(\lambda_1\mathbf{e}_1^T + \lambda_2\mathbf{e}_2^T\right)\mathbf{R}^{-1}, \tag{20}$$

where the Lagrange multipliers λ_1 and λ_2 are

$$\begin{aligned} \lambda_1 &= -\frac{\lambda_2\mathbf{e}_2^T\mathbf{R}^{-1}\mathbf{e}_1}{\mathbf{e}_1^T\mathbf{R}^{-1}\mathbf{e}_1}, \\ \lambda_2 &= \frac{2}{\left(\mathbf{e}_2^T - \frac{\mathbf{e}_2^T\mathbf{R}^{-1}\mathbf{e}_1}{\mathbf{e}_1^T\mathbf{R}^{-1}\mathbf{e}_1}\mathbf{e}_1^T\right)\mathbf{R}^{-1}\mathbf{e}_2}. \end{aligned} \tag{21}$$

3.3 | Standard digital correlated double sampling

In the standard digital correlated double sampling (CDS) readout process, the pixel charge is obtained subtracting the signal and pedestal mean values. Therefore samples in the transition between those levels are discarded. This is equivalent to having a filter

$$\mathbf{h}_{\mathbf{CDS}} = [\underbrace{-1/N, \cdots, -1/N}_{N}, \underbrace{0, \cdots, 0}_{L}, \underbrace{1/(N-L), \cdots, 1/(N-L)}_{(N-L)}]^T \tag{22}$$

with $N > L$, and L represents the number of samples discarded from the signal level to avoid the samples from the charge transient due to the exponential characteristic. Since the optimal filter will be compared to the CDS approach, we use N samples for the pedestal level and $N-L$ samples for the signal level thus both filter have the same total length and will use the same samples from the video signal to compute the pixel value. If N samples were used for the signal level of the CDS, additional samples not used for the optimal filter would be required. Due to the exponential behaviour of the charge signal, the pixel value obtained with digital CDS depends on the choice of L and N. Applying the filter (22) to equations (5) and (9), taking into account that the term $P\sum_{k=1}^{2N} h_k$ is zero because the sum of the CDS coefficients is zero, then, the expected pixel value, $E(P_Q)$, for the CDS is:

$$E(P_Q) = \sum_{k=1}^{2N} v_{o,iQ}[k]h_{CDS}[k] = \frac{\Delta V}{N-L}\sum_{k=N+1+L}^{2N}\left(1 - e^{-\frac{k-n_0}{n_1}}\right) = \frac{\Delta V}{N-L}\sum_{k=n_0+L}^{2N}\left(1 - e^{-\frac{k-n_0}{n_1}}\right) = \frac{\Delta V}{N-L}\sum_{k=L}^{N-1}\left(1 - e^{-\frac{k}{n_1}}\right), \tag{23}$$

where we used $n_0 = N+1$ and that $h_{CDS}[k] = 1/(N-L)$ for $k \geq n_0 + L$. It is possible to compute a closed form for the gain $g = E(P_Q)/\Delta$ of the digital CDS as:

$$g = E(P_Q)/\Delta V = 1 - \frac{e^{-\frac{(L-1)}{n_1}}}{(N-L)}\frac{\left(e^{-\frac{(N-L)}{n_1}} - 1\right)}{\left(1 - e^{1/n_1}\right)}. \tag{24}$$

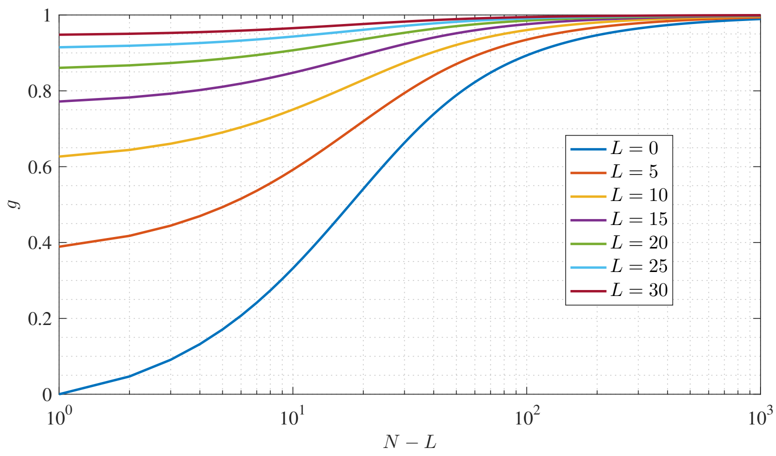

FIGURE 4 Gain g of the digital CDS filter as a function of $N - L$ for different values of width of the zero coefficients regions (L) and for a fixed time constant in samples $n_1 = 10.15$.

Equation (24) shows that the gain depends on the CDS parameters N and L and also on the time constant of the video signal in samples n_1. The value $E(P_Q)$ converges to ΔV when $N - L$ tends to infinity. For any practical situation $E(P_Q) < \Delta V$. This can be interpreted as an attenuation of the gain of the CDS filter.

Fig. 4 shows the gain as a function of $N - L$ for different values of L and for $n_1 = 10.15$. The lowest gain is obtained for small L and small $N - L$, since most of the signal samples used are from the transient time far from the settle time. Large L prevents low gain at the cost of longer readout times per pixel.

This gain g has an impact on the computation of the signal-to-noise ratio and should be considered for the comparisons with the optimal filter. It worth mentioning that for the optimal filter this gain g is always equal to 1 since in the optimization procedure the exponential shape is taken into account (see constraint for $\mathbf{e_2}$ in (14)) and the resultant filter coefficients weight the exponential samples in order to compensate the attenuation.

4 | SIMULATIONS AND COMPARISON TO PREVIOUS RESULTS

To simulate the results of the optimal filter under different practical situations, the effect of three types of noise were studied: (a) white noise, (b) quasi $1/f$ noise and (c) a linear combination of (a) and (b), representing three different idealized scenarios that could be found in CCD experiments. It is useful to give insight in how the optimal filter coefficients are shaped depending on the noise and also to compare the performance to the digital CDS.

First we generate an instance of normally distributed white noise $r_{white}[n]$ with zero mean and standard deviation of $\sigma_{white} = 1$. To generate quasi $1/f$ noise, $r_{1/f}[n]$, we filter another instance of white noise with a FIR filter designed using least-squares error minimization to approach a frequency response of the form $|H(e^{j\omega})| = 1/(1 + \omega/\omega_0)$ with $\omega_0/\pi = 0.5$ and $0 \leq \omega < \pi$. This response and the approximated FIR response are shown in Fig. 5(a), an attenuation of around 10 dB is expected in the quasi $1/f$ noise between the lower and higher frequencies. Because this would result in a noise with reduced variance (because of the energy lose due to filtering), we scale the noise to obtain an standard deviation of one: $\sigma_{1/f} = 1$. Finally, to obtain the combination of white and $1/f$ noise, we first compute $k \times r_{1/f}[n] + (1 - k) \times r_{white}[n]$, where $0 \leq k \leq 1$ is the percentage of $1/f$ noise, and then scale the result to obtain $\sigma_{1/f+white} = 1$.

In summary, the three types of noise are scaled such that all of them have the same standard deviation, which is the metric that we will use to evaluate the performance of the filters. The scaling of the standard deviation results in the Power Spectral Densities (PSD) of the simulated noises shown in Fig. 5(b). The white noise $r_{white}[n]$ has a constant power of -5 dB, $r_{1/f}[n]$ has an attenuation of 10 dB between its lower and higher frequencies, as expected from the frequency response of the filter shown in Fig. 5(a) and finally the combination of white noise and $1/f$ noise shows a PSD between the other two.

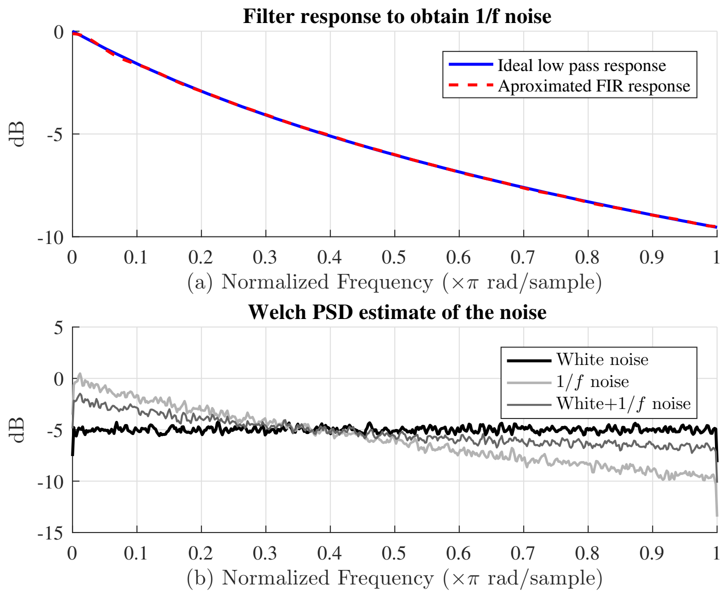

FIGURE 5 (a) Amplitude frequency response of $|H(e^{j\omega})| = 1/(1 + \omega/\omega_0)$ with $\omega_0/\pi = 0.5$ and $0 \le \omega < \pi$ used to generate $1/f$ noise; (b) Power Spectral Densities (PSD) of the simulated noises all scaled to have standard deviation equal to one.

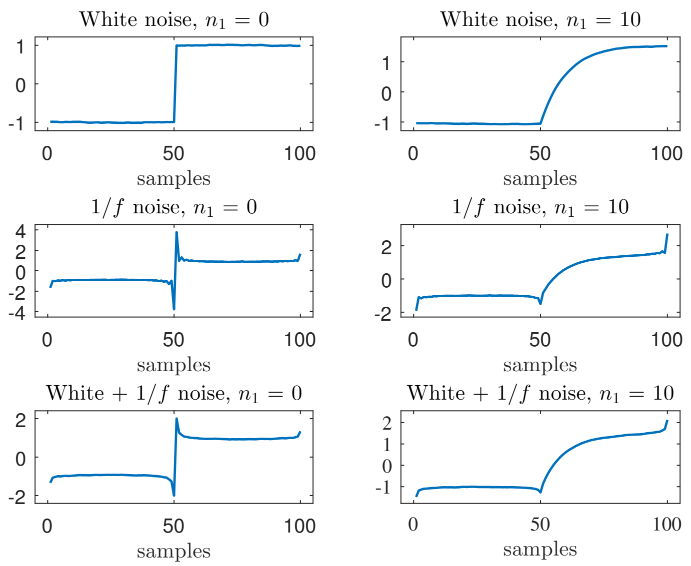

FIGURE 6 Shapes of the optimal digital filters scaled by N, obtained for the three types of noise (each row); considering instantaneous charge transfer ($n_1 = 0$, left column) and exponential charge transfer ($n_1 = 10$, right column).

4.1 | Shape of the optimal filters

Using the design equations (20) and (21) the coefficients of the filters for the three types of noise were computed. The instantaneous charge transfer $n_1 = 0$, and exponential charge transfer with time constant in samples equal to $n_1 = 10$ are considered. The results are summarized in Fig. 6 where the coefficients (scaled to N) are depicted with a continuous trace to expose their different shapes.

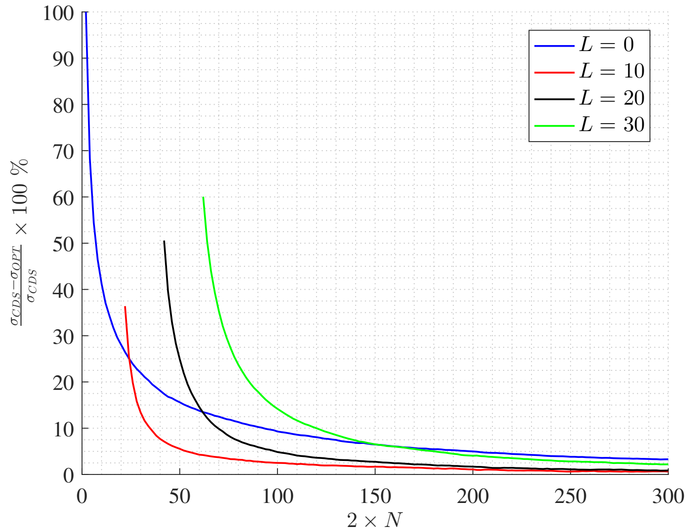

FIGURE 7 Simulated relative error reduction, comparing the standard deviation of the pixel noise computed with the proposed optimal filter and with the CDS using $L = 0, 10, 20, 30$ zero samples between pedestal and signal levels. With $N > L$.

For $n_1 = 0$ the results are in agreement with those reported in the literature by Stefanov[13,14] and Hegyi and Burrows[12] obtained using the "matched filter" theory. For pure white noise, the standard digital CDS technique (averaging the samples in the pedestal and signal level) is the optimal solution of the problem[12], this can be shown in Fig. 6 for white noise and $n_1 = 0$ where the scaled coefficients are approximately equal to ± 1 as in the digital CDS with $L = 0$ and coefficients scaled by N. Under quasi $1/f$ noise, results show that the filter coefficient heavily weights the samples within the transition almost implementing a backwards difference filter, which helps to remove the dominant low frequency noise present in this scenario. This filter is similar to that obtained by Gach et. al.[10] using simulated annealing optimization with the readout noise as cost function. Finally, to complete the $n_1 = 0$ scenario, the optimal solution for the combined noise results in "U" shaped coefficients for the pedestal and signal levels, with more amplitude in the central samples near the transition. This filter is a combination of the previous filters, which will be more similar to cases (a) or (b) depending on the amount of $1/f$ and or white noise.

The problem of considering instantaneous charge transfer ($n_1 = 0$) is that it is not practically feasible because even for fast CCDs system the charge and the video signal need certain number of samples to settle. The usual approach is to leave a gap between the pedestal and signal level (as explained in Section 3.3), but even a few sample dramatically deteriorates the performance of the optimal filter[14].

In the case of not-instantaneous charge transfer ($n_1 \neq 0$) the shape of the optimal filter coefficients are shown in the right column of Fig. 6 for $n_1 = 10$ samples and for each of the noise types. The shape of the filter coefficients reveal that the samples near the transition are weighted less than the final samples of the signal level, because the charge is not fully settled, similar to the behavior reported in[16] for the CCDs simulated under different noise conditions.

4.2 | Simulated performance of the optimal filter

The performance of the proposed technique compared to the digital CDS technique with L zero samples in the signal level was simulated under a 50% of white noise and 50% of $1/f$ noise scenario. The procedure is as follows: (a) an instance of the noise is generated and used to compute the auto-correlation of the noise; (b) the half-length N of the filters is swept from $N = L + 1$ to $N = 150$ while $L = 0, 10, 20, 30$ for the CDS; (c) the optimal filter and the CDS coefficients are computed for each value of N; (d) a new instance of noise, is generated for each N and used to compute the pixel values; (e) the process from (b)-(d) is repeated 100 times, storing all the pixel values in each repetition; (f) the standard deviation is computed for all the pixels computed with the same value of N.

The relative error reduction

$$\Delta\sigma = \frac{\sigma_{CDS} - \sigma_{OPT}}{\sigma_{CDS}} \times 100\%, \tag{25}$$

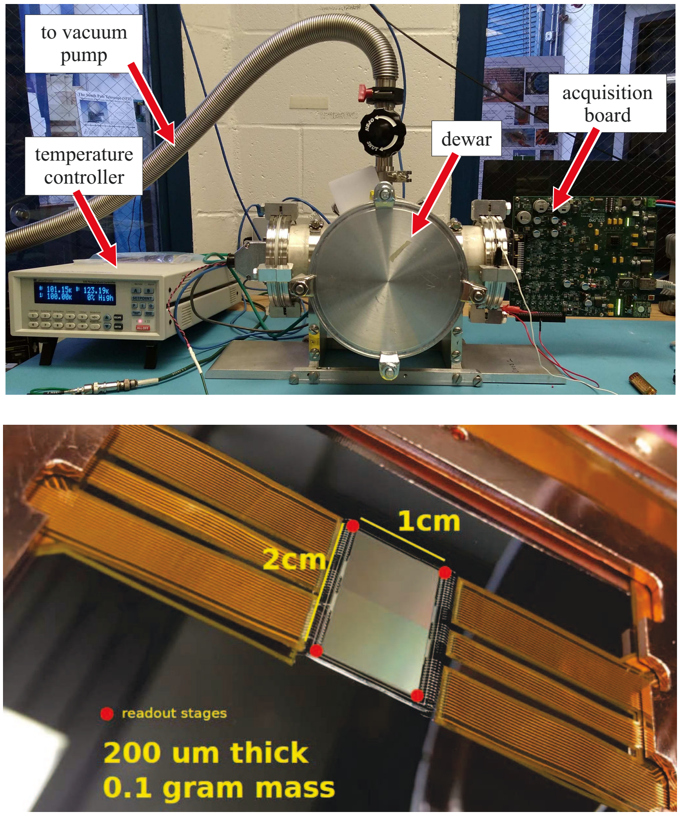

FIGURE 8 Experimental setup and CCD.

where σ_{OPT} is the standard deviation of the pixel noise computed with the optimal filter and σ_{CDS} computed with the CDS with a gap (L zero coefficients in the transition samples) is shown in Fig. 7. For this white and $1/f$ noise combinations, the error reduction is higher for short pixel times. The optimal filter outperforms the CDS since all the curves remain positive ($\sigma_{CDS} > \sigma_{OPT}$) in all the simulated region. This result also suggests, that an optimal value of L for the digital CDS could be found since the performance of the CDS is not monotonically increasing with the increase of L (the curves intersect). Experimental results are presented in the following section.

5 | EXPERIMENTAL RESULTS AND MEASUREMENTS

In this section we present experimental measurements which serve as a proof of concept towards the complete implementation of a CCD system based on an optimal filter that uses all the samples between the pedestal and signal levels.

Measurements were carried out using a 1248×724 pixels Skipper-type CCD [8,9]. The CCD is located inside a thick aluminum box (Dewar) at high vacuum (approximately 10^{-4} mbar) and at a temperature of 110 k. This low temperature setup (typical in CCDs applications) is used to minimize thermal noise (also known as Johnson-Nyquist noise) which is generated by the thermal agitation of charge carriers. The high vacuum is necessary to avoid water condensation at low temperature.

The readout electronics was developed by the research group [20] and allows to capture raw video signals before computing the pixel values. Fig. 8 shows a photograph of the experimental setup where all instruments have been labeled, and also a photograph of the CCD. Red dots indicate the location of the four output stages. The data processing and control of the peripheral components is done by the Artix-7 FPGA (XC7A200T). Bias voltage together with clock generation units create the signals that are necessary to drive the CCD, which integrates four output video channels. These video signals are digitized using 18-bit, 15 MSPS analog-to-digital converters (ADC, LTC2387) based on successive approximation registers (SAR), tightly coupled with low-noise differential operational amplifiers (LTC6363). Output samples of the converters are fed into the FPGA to perform

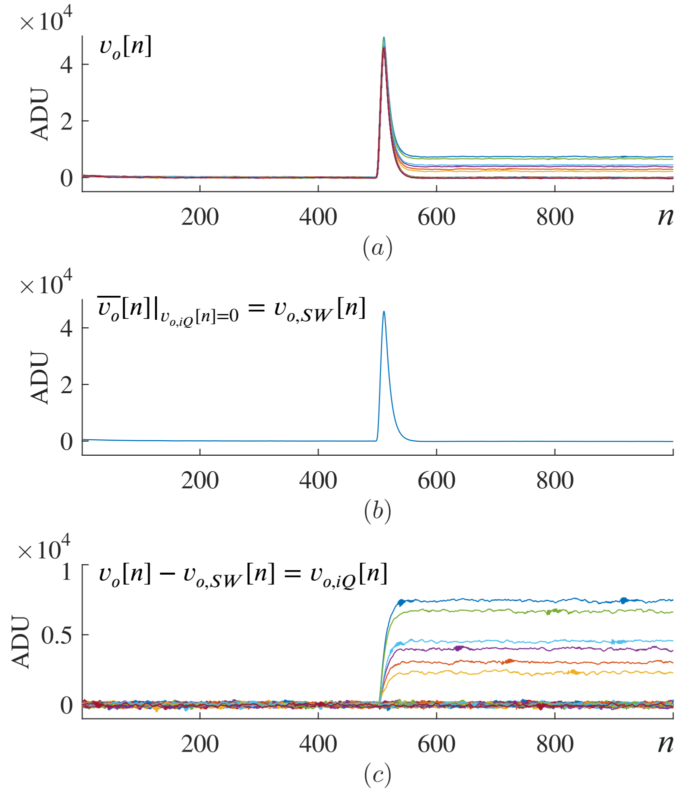

FIGURE 9 Measured charge transfer in the video signal. (a) Various pixels overlapped, $v_o[n]$ with and without charge; (b) average of the empty pixels (i.e., zero charge pixels) in Fig. (a), resulting in a measurement of the Summing Well signal $v_{o,SW}[n]$; (c) pixels in Fig. (a) with average pixel in Fig. (b) subtracted resulting in a measurement of the charge signal $v_{o,iQ}[n]$.

digital filtering and image reconstruction. The user interacts with the board through a single Ethernet port, which allows sending and receiving commands as well as data.

5.1 | Charge transfer measurements

The measured video signal $v_o[n]$ with 10^3 acquired raw samples (before the pixel computation) at a sampling frequency of $F_s = 1/T_s = 15$MHz is shown in Fig. 9. In Fig. 9(a) several pixels with and without charge are overlapped. The pedestal level P of each pixel was computed by averaging the first N samples and this value was subtracted from each pixel. The signal $v_{o,SW}[n]$ is obtained by averaging the empty pixels of Fig. 9(a), where $\Delta V = 0$, and is shown in Fig. 9(b). Finally, the signals $v_{o,iQ}[n]$ were obtained by subtracting the averaged pixel in Fig. 9(b) to the pixels in Fig. 9(a) and are depicted in Fig. 9(c).

Measurements shown in Fig. 9(c) confirm the exponential nature of the charge transfer and the Summing Well (SW) feedthrough assumptions. This is an important proof of concept for the optimal filter since it was possible to decouple the feedthrough and charge dynamics using experimental measurements as it was modeled in Section 2.

The only parameter from (3) necessary to compute the filter coefficients is the time constant τ, which in samples is n_1. This is relevant to determine $\mathbf{e_2}$, since n_1 is obtained as the ratio between τ and the sampling period T_s. Charge signals $v_{o,iQ}[n]$ in Fig. 9(c) were fitted with an exponential to find that the time constant in samples is $n_1 = 10.15$. Fig. 9(c) also shows that the instant at which the charge transfer occurs is $n_0 = 500$, giving $t_0 = 500T_s = 33.3\mu$s.

5.2 | Computing the filter coefficients and computational complexity

Table 1 list several steps that should be followed to compute the optimal filter for a given experimental setup. Specifically, we propose and experimentally verify the following method to measure the system noise for the calculation of the auto-correlation.

First, M samples of the video signal in which no clocking of any signal of the CCD occurs have to be acquired (noise-only samples). A correct polarization of the built-in CCD's output amplifier is required to ensure that when the noise is acquired, the output stage is operating at the same bias point that in normal operation (when the CCD is readout). To achieve this condition, we propose to use the standard clocking sequence but extend the pedestal interval to more than M samples and use these pedestal samples to capture the system's noise. This could be the best practical option in any experimental setup for two reasons: (1) almost every CCD readout system has the option of customizing the timing of the sequencer and therefore it is easy to extend the pedestal interval. No additional modification of the reading sequence is needed; (2) keeping the standard clocking sequence and using a longer pedestal as noise samples is a good representation of the noise under actual working conditions because before the pedestal interval, the sense node is reset and the gate of the output amplifier is at a known voltage. Moreover, all other voltages applied in a standard reading are still applied during noise measurement, so any capacitively coupled noise is also present, resulting in the same operational condition of the output stage of the CCD.

Fig. 10 shows the filter coefficients computed by solving (20) for different values of N. The optimal filter coefficients show two relevant features: high coefficients values at the beginning, center and at the end, which are responsible of a better correlated noise ($1/f$) rejection. The rest of the coefficients have an almost constant value, allowing white noise reduction. This characteristic is more clearly represented for the filter with $N = 500$ and $N = 700$.

The computational complexity of the algorithm can be splited in two parts: 1) computation of the coefficients, which is only performed occasionally, when a new experiment is setup or when the experimental and/or environmental conditions change in such a way that there is an impact in the noise of the system: for example a change of CCD would probably required a re-computation of the optimal filter coefficients. The computation of the filter is done off-line and can be programmed as a built-in software routine that the user can call. The most computationally intensive part is the inverse of the matrix auto-correlation (which may be computed using iterative or computational efficient methods) but this routine is not time critical since it is only computed sporadically and not in normal operation when images are being acquired; 2) computation of the pixel values using the optimal filter, which is time-critical because it is necessary for computing the value of every pixel. It is computed in the FPGA using a multiply and accumulate structure (MAC structure like for FIR filtering) and a $4N$ samples memory bank ($2N$ registers for the coefficients and $2N$ registers for the video signal samples). The standard readout technique (digitla CDS) can be implemented with lower memory requirements, using only a scaled signed accumulator: the digital CDS can be thought as a scaled FIR filter with coefficients ± 1. Although optimal filter computation seems more intensive, modern FPGAs include IP blocks specifically designed to implement these type of filters with maximum efficiency and minimum software overhead. The increase in complexity is minimal compared with the benefit obtained in noise reduction.

5.3 | Noise scan

A typical performance test to evaluate CCD detectors and its electronics is the measurement of the noise scan[19], i.e., the computation of the noise standard deviation as a function of the pixel readout time (in our case, as a function of the filter length $2N$). The RMS noise as a function of the total filter length was computed for both the standard CDS and the proposed optimal filter. A noise-only CCD signal, without pixel structure, was acquired and processed. This allows to measure and understand to a full extent the capabilities and advantages of the optimal filter compared to the CDS. Some hardware issues may condition the performance of the filter, for example, if the video signal averaged in Fig. 9(b) are not sampled at the same time instant for every pixel.

A PSD of the measured noise is shown in Fig. 11. The system noise has a dominant $1/f$ component of more than 90% of $1/f$ over white noise. However, the real noise is not only a perfect combination of $1/f$ noise and white noise as in the simulated scenario presented in Section 4, because the spectrum contains several spikes and spectral regrowth. Those effects can be introduced by the electronics (for example due to switching power supplies), long wiring, environmental condition, etc.

Notice that the video signal takes around $L = 30 \approx 3 \times n_1$ samples to achieve the almost constant signal level (see Fig. 9). Results of the noise scan are shown in Fig. 12 where the pixel variance for CDS (parametrized for $L = 0$, $L = 10$, $L = 20$, $L = 30$) and the optimal filter are plotted as a function of the total filter length $2N$ and considering $N > L$ for the CDS. The pixel error with the optimal filter is always lower than the pixel error for the CDS for any value of L and for every value of total filter length, showing the benefits of the optimal filter for any pixel time.

The relative reduction of the noise variance for the optimal filter in comparison with CDS for different L values is shown in Fig. 13, where we plot the percentual $\Delta\sigma = 100 \times (\sigma_{CDS} - \sigma_{OPT})/\sigma_{CDS}$ as a function of the filter length $2N$ parametrized for

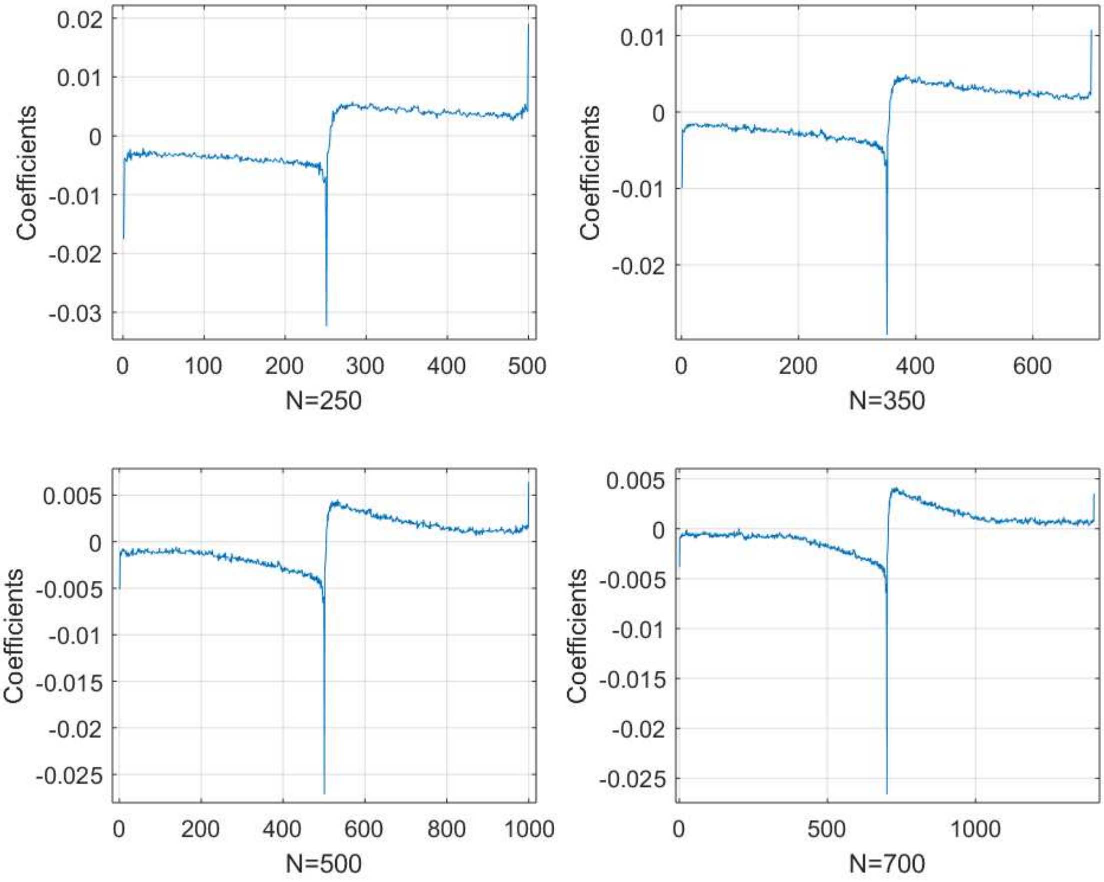

FIGURE 10 Optimal filter coefficients for $N = 250$, 350, 500 and 700 obtained for the measured noise.

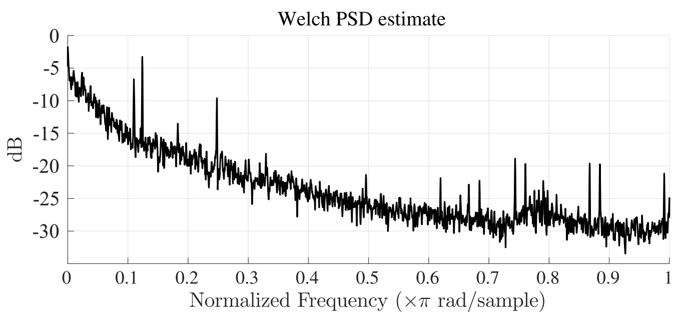

FIGURE 11 Power Spectral Densities (PSD) of the measured noise in the experimental setup.

different L values of the CDS filter. In any case $\Delta\sigma$ is always positive, i. e., σ_{OPT} is lower than σ_{CDS} revealing that the optimal filter outperforms the CDS, and the improvement is more noticeable (more than 10%) for fast CCD readouts (i.e, low $2N$ values).

5.4 | Final Discussion

A previous theoretical development to compute an optimal filter that takes into account the transition samples ($n_1 \neq 0$) was reported by Alessandri et. al.[16], where an exponential characteristic associated to the limited bandwidth of the video signal

1) Pure noise measurement:
Acquire a number $j = 1 \cdots M$ of raw video signal samples of pure noise $v_\eta[j]$. In these M samples there should be no clocking of any signal of the CCD. This noise must be representative of the actual noise present during CCD operation. These implies that the output stage of the CCD should be polarized at the same bias point, to do so we propose to: *a*) Extend the pedestal interval to more than M samples. *b*) Use these pedestal samples as the noise, this has the advantage that prior to the pedestal interval the Sense Node (SN) is reset and hence the gate of the output transistor is at a a known voltage. Moreover, all other voltages applied in a standard reading are still applied during noise measurement, so any capacitive noise coupling is also present.
2) Pre-process the noise:
If necessary, remove any DC offset or trend added by the acquisition software/hardware.
3) Estimate the noise auto-correlation:
For example, the element u of the auto-correlation vector as $$R_\ell[u] = \frac{1}{M}\sum_{j=1}^{M-u} v_\eta[j+u]v_\eta[j]$$ where ℓ is the maximum estimated lag (required filter length), $u = 1 \cdots \ell$ and $M \gg \ell$ to avoid any bias in the estimator.
4) Build the auto-correlation matrix R:
Form a vector with elements $\mathbf{R}_\ell = [R_\ell[1], R_\ell[2]] \cdots R_\ell[\ell]]$, to generate $\mathbf{R}$ as the Toeplitz matrix of the vector $\mathbf{R}_\ell$.
5) Identify the time constant:
Find n_1 of the video signal in samples.
6) Compute the optimization constraints vectors:
Compute $\mathbf{e}_1$ and $\mathbf{e}_2$ vectors as indicated in (11) and (12).
7) Compute the filter coefficients:
Compute $\mathbf{h}$ using (20) and (21).

TABLE 1 Experimental steps to compute the optimal filter

was proposed and results were verified by simulation. We have extended this analysis by adding a detailed modeling of the charge transfer characteristic in the output stage of the CCD including the video signal feedthroughs, which is confirmed by he experimental results shown in Fig. 9. We also developed an experimental approach to compute the optimal filter coefficients by measuring the setup noise that is representative of the system noise during normal operation. The complete pixel structure or average pixel (Fig. 9.b) was not included in the noise scan measurements. In this way, the lack of the hardware capability of synchronized pixel sampling does not affect the noise reduction capabilities of the optimal filter. Future work will focus on computing the pixel values using the complete pixel structure, which requires precise synchronization between the sequencer that operates the CCD and the digital acquisition of the video signal samples.

Both Fig. 12 and 13 suggests, in coincidence with the simulation section, that due to the behaviour of the noise with L, an optimal value of L for the digital CDS could be found, this optimization is out of the scope of this work, but recent studies analyse this type of optimization [11].

Measurements also show that the proposed optimal filter outperforms the CDS in all cases with the advantage been more noticeable for low values of $2N$ which is equivalent to faster readouts, even a percentage of noise reduction of 10% can result in great science improvements for some areas such as astronomy for high resolution spectroscopy or exoplanets detection or in particle detection applications.

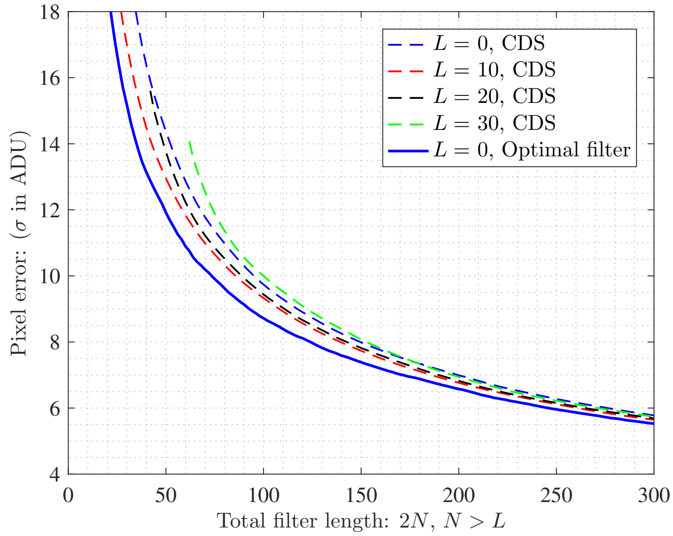

FIGURE 12 Noise scan: pixel error (standard deviation σ in ADU) as a function of $2N$ for the digital CDS and optimal filter. Measurements obtained with actual noise of the experimental setup.

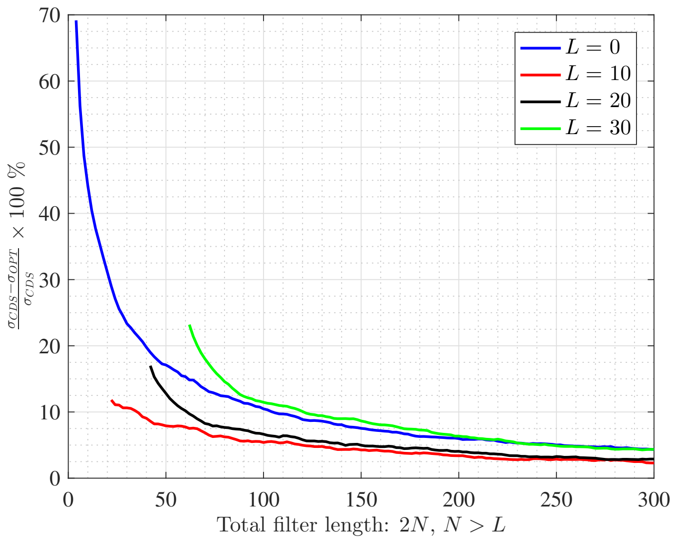

FIGURE 13 Relative noise reduction $(\sigma_{CDS} - \sigma_{OPT})/\sigma_{CDS}$ as a function of the filter length $2N$ parametrized for different L values of the CDS filter. Measurements obtained with actual noise of the experimental setup.

6 | CONCLUSION

A detailed modeling of the video signal and charge transfer characteristic of the output stage of the CCD were presented, including the modeling of the clock feedthroughs. An optimal filter to compute the pixel values which takes into account the charge transfer characteristic in CCD readout and noise characteristic was developed. It considers all the samples in the readout, even those in the transition between pedestal and signal levels. The proposed technique gives better noise rejection than the CDS technique for the same filter length or equivalently, a reduction of the pixel-time for the same readout noise. The relative performance of both methods was compared showing that the optimal filter outperforms the standard CDS in more than 10 % for fast CCD readouts. A practical recipe to compute the coefficients of the digital filter using closed form expressions was given.

References

1. Teymouri M, Sobhi J. An ultra-linear CMOS image sensor for a high-accuracy imaging system. *International Journal of Circuit Theory and Applications* 2018; 46(9): 1593–1605.

2. Katic N, Kamal MH, Schmid A, Vandergheynst P, Leblebici Y. Compressive image acquisition in modern CMOS IC design. *International Journal of Circuit Theory and Applications* 2015; 43(6): 722–741.

3. Nascetti A. Fractional charge packet counting with constant relative resolution. *International Journal of Circuit Theory and Applications* 2012; 40(2): 175–187.

4. Sá dLB, Dias MHC, Dupret A, Mesquita Filho dAC. A 99.95% linearity readout circuit with 72 dB dynamic range for active pixel sensors. *International Journal of Circuit Theory and Applications* 2018; 46(9): 1580–1592.

5. Leñero-Bardallo JA, Carmona-Galán R, Rodríguez-Vázquez A. Applications of event-based image sensors-Review and analysis. *International Journal of Circuit Theory and Applications* 2018; 46(9): 1620–1630.

6. Aghamousa A, Aguilar J, Ahlen S, et al. The DESI Experiment Part I: Science, Targeting, and Survey Design. *arXiv preprint arXiv:1611.00036* 2016.

7. Marshall P, Anguita T, Bianco FB, et al. Science-driven optimization of the LSST observing strategy. *arXiv preprint arXiv:1708.04058* 2017.

8. Fernández Moroni G, Estrada J, Cancelo G, Holland SE, Paolini EE, Diehl HT. Sub-electron readout noise in a Skipper CCD fabricated on high resistivity silicon. *Experimental Astronomy* 2012; 34(1): 43–64. doi: 10.1007/s10686-012-9298-x

9. Tiffenberg J, Sofo-Haro M, Drlica-Wagner A, et al. Single-electron and single-photon sensitivity with a silicon Skipper CCD. *Phys. Rev. Lett.* 2017; 119: 131802. doi: 10.1103/PhysRevLett.119.131802

10. Gach JL, Darson D, Guillaume C, et al. A new digital CCD readout technique for ultra-low-noise CCDs. *Publications of the Astronomical Society of the Pacific* 2003; 115(811): 1068.

11. Weatherill DP, Shipsey I, Arndt K, et al. Automatic selection of correlated double sampling timing parameters. *Journal of Astronomical Telescopes, Instruments, and Systems* 2019; 5(4): 1 – 8. doi: 10.1117/1.JATIS.5.4.041502

12. Hegyi DJ, Burrows A. Optimal sampling of charge-coupled devices. *The Astronomical Journal* 1980; 85: 1421–1424.

13. Stefanov K, Murray N. Optimal digital correlated double sampling for CCD signals. *Electronics Letters* 2014; 50(14): 1022–1024.

14. Stefanov KD. Digital CDS for image sensors with dominant white and 1/f noise. *Journal of Instrumentation* 2015; 10(04): P04003.

15. Simbeni PQ, Moroni GF, Chierchie F, et al. Optimal filter for noise reduction in CCD readout. In: XVII Workshop on Information Processing and Control (RPIC). ; 2017: 1-5

16. Alessandri C, Abusleme A, Guzman D, Passalacqua I, Alvarez-Fontecilla E, Guarini M. Optimal CCD readout by digital correlated double sampling. *Monthly Notices of the Royal Astronomical Society* 2016; 455(2): 1443-1450.

17. Simbeni PQ, Moroni GF, Chierchie F, et al. Optimal filter design considering charge transfer characteristics for CCD readout. In: 2019 Argentine Conference on Electronics (CAE). IEEE. ; 2019: 41-46

18. Holland S, Groom D, Palaio N, Stover R, Wei M. Fully depleted, back-illuminated charge-coupled devices fabricated on high-resistivity silicon. *IEEE Transactions on Electron Devices* 2003; 50(1): 225-238. doi: 10.1109/TED.2002.806476

19. Janesick JR. *Scientific charge-coupled devices*. 83. SPIE press . 2001.

20. Moroni GF, Chierchie F, Haro MS, et al. Low threshold acquisition controller for skipper charge coupled devices. In: 2019 Argentine Conference on Electronics (CAE). IEEE. ; 2019: 86–91.